Journal of Materials Chemistry A

Accepted Manuscript

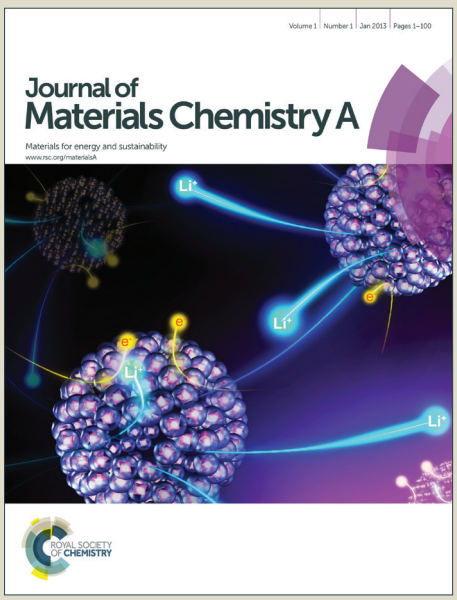

ROYAL SOCIETY OF CHEMISTRY

www.rsc.org/materialsA

Journal of Materials Chemistry A

RSCPublishing

ARTICLE

Fabrication of Antifouling Polymer-Inorganic Hybrid Membranes through Synergy of Biomimetic Mineralization and Nonsolvent Induced Phase Separation

Cite this: DOI: 10.1039/x0xx00000x

Received 00th January 2012,
Accepted 00th January 2012

DOI: 10.1039/x0xx00000x

www.rsc.org/

Xueting Zhao[a,b], Yanlei Su[a,b], Jialin Cao[a,b], Yafei Li[a,b], Runnan Zhang[a,b], Yanan Liu[a,b], and Zhongyi Jiang[a,b,*]

Membrane-based technology is regarded as the most promising approach for oil/water separation, but suffers from the severe membrane fouling. Hybrid membranes may win rich opportunities in dealing with fouling problem due to their hierarchical structure and multiple functionalities. In this study, novel kinds of hybrid membranes with both inorganic hydrophilic microdomains and organic low surface free energy (LSFE) microdomains are fabricated through the synergy of *in situ* biomimetic mineralization and nonsolvent induced phase separation. The as-prepared hybrid membrane possesses homogeneous dispersion of nanoparticles, higher mechanical strength, underwater superoleophobicity and surface heterogeneousity. Owing to the concomitant collaborative fouling-resistant mechanism and fouling-release mechanism, the oil foulants are difficult to arrive at or attach to the membrane surface, and consequently the membranes display significantly enhanced antifouling property and separation performance. Particularly, the permeation flux decline closes to zero during oil-in-water emulsion filtration. This study may endeavor a facile and generic strategy to manipulate the structure-property relationship of membranes for efficient water treatment processes.

Introduction

Millions of tons of oily wastewater are generated daily around the world. Primary sources of oily wastewater are from industrial processes, such as oil and gas extraction, oil refining, petrochemical, food, steelmaking, and leather manufacturing. Accordingly, the ever-increasing industrial oily wastewater with high pollution load has become severe environmental and health issues.[1-3] Due to the green, energy-saving, and continuous operation feature, membrane-based oil/water separation technologies have evolved an economical and efficient approach to concentrate and remove oil from water. However, the inherent oil fouling often triggers a cascade of events such as accumulation, adhesion, spreading, coalescing and migration of suspended oil foulants, which is much more complicated than the fouling caused by soluble organic macromolecules and insoluble inorganic matters. When oil droplets are rejected and directly contact with membrane surfaces, the hydrophobic interaction between oil droplets and membrane surfaces renders the relatively low interfacial free energy of oil/membrane interface. As a result, the increasing difference in the interfacial free energies between water/membrane and oil/membrane interfaces ($\gamma_{W\text{-}M}$-$\gamma_{O\text{-}M}$) facilities the wetting and spreading of oil droplets on the surface as predicted by Young's equation (Scheme 1). The gradual coalescing and migration of oil droplets form continuous oil film and cause sharp decline of permeation flux temporarily or permanently.

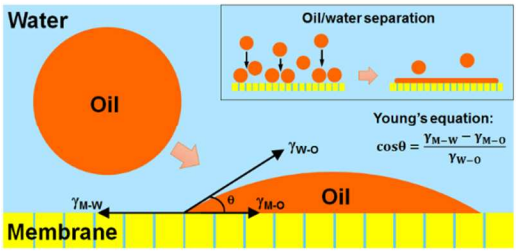

Scheme 1 Wetting behaviors of oil droplets on membrane surface (Young's mode in membrane/oil/water three-phase systems).

In order to achieve anti-oil-fouling membrane materials for efficient oil/water separation, different functional materials with specific chemical or geometrical structures have been exploited to effectively suppress the hydrophobic interactions

between oil droplets and membrane surfaces. These materials include organic materials (polymer brushes[4-18] and polymer nanomaterials[19]), inorganic materials (metal compounds[8, 20-23], silicon-based materials[24, 25], carbon-based materials[16, 18, 22, 23, 26-28]) and hybrid materials[29]. The core of anti-oil-fouling strategy lies in the construction of powerful defense mechanisms. According to fouling-resistant mechanism, water molecules tightly surrounding the hydrophilic surfaces decreases the possibility of direct hydrophobic interactions.[30, 31] According to fouling-release mechanism, strongly electronegative fluorine atoms on low surface free energy (LSFE) surfaces decrease the susceptibility to hydrophobic interactions.[32, 33] Accompanying the switch of antifouling strategy from single defense mechanism to multiple defense mechanisms, the recent efforts have begun to focus on heterogeneous membrane materials with both hydrophilic and LSFE microdomains.[8, 11-14, 29] Still, one great challenge is how to achieve the reliable creation of collaborative defense mechanisms based on the rational design of membrane materials and formation methods. It is worth noting that, polymer-inorganic hybrid membranes, featured by hierarchical structures and multiple functionalities, will win rich opportunities in manipulating collaborative defense mechanisms.

When preparing the polymer-inorganic hybrid membranes, homogeneous dispersion of inorganics, good interface compatibility between polymer and inorganics are two essential issues. Fortunately, biomineralization renders an exceptional solution in which organisms produce hard inorganic materials within organic macromolecular matrixes under ambient temperature, near neutral pH and in aqueous solution. The formation of natural organic-inorganic hybrid materials, such as shells, pearls, and bones, includes self-assembly of organic matrixes and subsequent orientation, nucleation, and growth of biominerals.[34-36] Deriving from the basic principles of biomineralization, biomimetic mineralization opens a facile avenue to artificial organic-inorganic hybrid materials with complex structures. In this process, inorganic materials with controlled dispersion, tunable size and hierarchical morphology are generated *in situ* in organic matrix.[37-39] Organic matrixes (natural proteins, peptides or amino acids and synthetic polyamines) not only act as structural templates and confined compartments, but also play pivotal roles in catalyzing the nucleation and growth of inorganics.[40] Since biomimetic mineralization takes place *in situ* within organic matrixes, hybrid materials can not only possess homogeneous dispersion of inorganics, good interface compatibility between polymer and inorganics, but also avoid the drawbacks of severe aggregation or harsh conditions in physical blending and sol-gel methods.[34, 41-43] Based on the rapid progress of biomimetic mineralization, some nonporous polymer-inorganic hybrid membranes for sustainable energy applications has been fabricated through *in situ* biomimetic mineralization method either by utilizing membrane-forming polymer with mineralization ability[41, 44] or *in situ* incorporating additional mineralization into membrane-forming polymer matrix.[45] These hybrid membranes offer a number of benefits due to the combined physicochemical properties from both polymers and inorganics, such as tunable multiple interactions and hierarchical structure, improved interfacial morphology, and optimal free volume and mass transfer characteristics. However, rare studies have employed *in situ* biomimetic mineralization method to prepare polymer-inorganic hybrid membranes for sustainable water treatment applications. It can be envisioned that biomimetic mineralization method may take advantage of the synergistic benefit of polymer and inorganics, and provide a promising toolbox for creating collaborative defense mechanisms on membrane surface.

Herein, we explored a novel method for preparing polymer-inorganic hybrid membranes through the synergy of biomimetic mineralization and nonsolvent induced phase separation. Synthetic polyamines grafted on polymer matrix induce the *in situ* growth and organization of inorganic nanoparticles (NPs). Accordingly, the as-prepared hybrid membranes manifest the distinct advantages, such as homogeneous NPs dispersion, high mechanical strength, and underwater superoleophobicity. More importantly, when LSFE moieties are selectively decorated on hydrophilic nanoparticle surface or polymer side chains, the hybrid membranes were endowed with collaborative defense mechanisms for the efficient separation of oil-in-water emulsion, effectively avoiding foulants from approaching and attaching to the surfaces. The practicality of such heterogeneously constructed hybrid membranes will emerge attractive prospects for oily wastewater treatment.

Experimental

Synthesis of PVDF-g-PTA copolymer

Poly(vinylidene fluoride) (PVDF, FR-904, Shanghai 3F New Material Co. Ltd) was first immersed and high-speed stirred in potassium hydroxide solutions (KOH, 10.0 wt%, H_2O 89.9 wt%, and 0.1 wt% ethanol) at 60 ^oC for 30 min (hydrofluoric acid elimination reaction of PVDF induces the formation of double bonds for subsequent polymerization), and then the product PVDF(-HF) was washed with distilled water to neutrality and dried under vacuum. PVDF(-HF) (4.0 g) was dissolved in *N,N*-dimethylformamide (DMF, 50 ml) and degassed completely by with nitrogen. Then, the monomer [2-(methacryloyloxy)ethyl]trimethylammonium chloride (TA, 80 wt% in aqueous solution, 20mmol, Aldrich Chemical Co.) was added to the system and polymerized with PVDF(-HF) at 70 ^oC using 2,2'-azobis(2-methylpropionitrile) (AIBN, 1 mmol, Tianjin Guangfu Fine Chemical Research Institute) as initiator (the synthetic scheme is shown in Fig. S1†). After 12 h, the reaction solution was precipitated in ethanol and washed four times with ethanol to remove residue monomer, homopolymer and initiator. The resulting PVDF-g-PTA copolymer was dried by freeze-drying for 12 h for membrane preparation. The chemical composition of PVDF-g-PTA copolymer were characterized by attenuated total reflection Fourier transform infrared spectroscopy (ATR-FTIR, Bruker VERTEX 70) and Thermogravimetric analysis (TGA, NETZSCH TG209 F3, O_2 atmosphere).

Synthesis of PVDF-g-xPHFBM-PTA copolymer

The PVDF-g-xPHFBM-PTA copolymer was synthetized by a procedure similar to that described above. PVDF(-HF) (4.0 g) was dissolved in DMF (50 ml). The monomer 2,2,3,4,4,4-hexafluorobutyl methacrylate (HFBM, 10 or 20 mmol, Xeogia Fluorine-Silicon Chemical Co. Ltd.) was added to this solution at 70 ^{o}C under nitrogen and polymerized with PVDF(-HF) at the same temperature for 2 h, initiated by AIBN (1 mmol). Subsequently, the monomer TA (20mmol) was added dropwise to the system, polymerized for another 10 h, and then poured into ethanol to precipitation. The resulting PVDF-g-xPHFBM-PTA copolymer (x=0.5, 1) was throughout washed and dried by freeze-drying for 12 h for membrane preparation. The chemical composition of PVDF-g-xPHFBM-PTA copolymer was characterized by ATR-FTIR (Bruker VERTEX 70).

Synthesis of fluorinated triethoxysilane precursor

Fluorinated triethoxysilane precursors was prepared by michael addition according to the literature procedures.[46] Briefly, 2,2,3,4,4,4-hexafluorobutyl acrylate (HFBA, 4.7 g, 19.8 mmol, Xeogia Fluorine-Silicon Chemical Co. Ltd.) was added dropwise into (3-aminopropyl)triethoxysilane (APTS, 2.0 g, 9.0 mmol, Heowns Biochem LLC) in an ice bath. Then the ice bath was removed and stirring was continued for another 24 h at 80 ^{o}C. The excess amounts of HFBA were removed under a vacuum, yielding HFBA-based triethoxysilane (FTS) precursor. The chemical composition of FTS precursor was characterized by FTIR (Bruker VERTEX 70).

Membrane preparation and characterizations

PVDF-g-PTA/TiO_2 hybrid membranes were fabricated by *in situ* biomimetic mineralization. PVDF-g-PTA (12 wt%) was dissolved in NMP at 60 ^{o}C, forming homogenous and transparent solutions. Then, the precursor Titanium(IV) bis(ammonium lactato)dihydroxide (TALH, 50 wt% in aqueous solution, Aldrich) was slowly added dropwise to the PVDF-g-PTA/NMP system with rapid stirring. The biomimetic mineralization took place in a few seconds and the solutions turned to white and opaque (Fig. S4†). The theoretical content of generated TiO_2 NPs calculated from the initial composition were designed to be 2.5, 5 and 10 wt% *versus* the weight of PVDF-g-PTA, assuming 100% conversion of the precursor. After stirring for 12 h, the resulting casting solutions were degassed at the same temperature for another 12 h, and then cooled to room temperature. Afterwards the solutions were cast onto a glass plate using a casting knife with 240 μm gap height, and converted into asymmetric hybrid membranes via nonsolvent induced phase separation (25 ^{o}C water bath). The detached membranes were stored in deionized water before use.

Two kind of hybrid membranes with heterogeneous surface chemistries were prepared: (a) PVDF-g-xPHFBM-PTA/TiO_2 hybrid membranes (x=0.5, 1) were fabricated similar to that described above for the PVDF-g-PTA/TiO_2 hybrid membranes. PVDF-g-xPHFBM-PTA (12 wt%) was utilized as membrane-forming polymer and inducers of TALH (10 wt% theoretical content of generated TiO_2 NPs *versus* the weight of PVDF-g-xPHFBM-PTA). The degassing, casting, and coagulating processes were the same as above; (b) PVDF-g-PTA/TiO_2-xFTS hybrid membranes (x=0.5, 1) were fabricated by coupling the *in situ* generated TiO_2 surface with FTS precursors. After 12 h of mineralization in the PVDF-g-PTA/NMP/TALH system, FTS precursors (0.5 or 1 weight equivalent of theoretical TiO_2 content) was added dropwise and condensation for another 12 h. The degassing, casting, and coagulating processes were the same as above. PVDF-g-PTA membrane and PVDF-g-PHFBM-PTA membrane were also prepared as control membranes from the casting solution with 12 wt% membrane-forming polymers in NMP.

The surface and cross-section morphologies of membranes were observed with scanning electron microscopy (SEM, FEI Nova Nanosem 430). The surface chemistries of membranes were characterized by X-ray photoelectron spectroscopy (XPS, Kratos Axis Ultra DLD) and energy-dispersive X-ray (EDX, Oxford INCA Energy). The actual contents of *in situ* generated TiO_2 NPs were determined by thermogravimetric analysis (TGA, NETZSCH TG209 F3, air atmosphere) equipment. The morphology of generated TiO_2 NPs were observed with transmission electron microscope (TEM, JEM-2100F) after removing organic matters by calcination. The mechanical properties of membranes were tested by tensile testing machine (Testometric AXM350-10KN). The contact angles of water (or diiodomethane) sessile drop (5 μL) and underwater air (or oil) captive bubble (10 μL) on membrane surfaces were characterized by contact angle goniometer (JC2000C Contact Angle Meter).The total surface free energy (SFE, γ_s) of membrane surfaces, as well as the polar (γ_s^p) and dispersive (γ_s^d) components, were calculated from the two-liquid methods of Owens and Wendt,[47] employing water as polar test liquid and diiodomethane (CH_2I_2) as nonpolar test liquid.

Oil-in-water emulsion filtration and antifouling property evaluation

Surfactant-stabilized oil-in-water emulsion (GS-1 high-speed vacuum oil 0.9 g L^{-1} and SDS 0.1 g L^{-1}, average diameter ~2.1μm) was employed as the model foulant solution. Separation of the oil-in-water emulsion was performed on a dead-end stirred cell (effective membrane area of 28.7 cm^2) connected with a solution reservoir and nitrogen gas cylinder. The transmembrane pressure was controlled at 0.05 MPa by pressurized nitrogen gas and stirring speed was locked at 200 rpm by magnetic stirrer. Each membrane was first pre-compacted at 0.1MPa with distilled water, and then underwent 0.5 h filtration of distilled water and subsequent 1 h filtration of oil-in-water emulsion. After the separation of oil-in-water emulsion, 0.5 h hydraulic rinsing of membranes was carried out, followed by another 0.5 h filtration of distilled water. The permeate fluxes J (L/(m^2 h)) for each membrane in different stages were calculated to evaluate the antifouling properties according to:

$$J=\frac{V}{A\Delta T}$$

with V (L) being the volume of permeated water, A (m^2) being the effective membrane area, and ΔT (h) being the time span between measurements. For antifouling property evaluation, the initial permeate fluxes of water (J_{w1}), the finial permeate fluxes of oil-in-water emulsion (J_o), and the permeate fluxes of cleaned membrane (J_{w2}) were analyzed in detail: total flux decline ratio (DR_t=1-J_o/J_{w1}), reversible flux decline ratio (DR_r=(J_{w2}-J_o)/J_{w1}), irreversible flux decline ratio (DR_{ir}=1-J_{w2}/J_{w1}), and flux recovery ratio (FRR=J_{w2}/J_{w1}). In general, the inhibition of flux decline and improvement of flux recovery indicated better antifouling properties of membranes.

Results and discussion

Preparation of hybrid membranes via *in situ* biomimetic mineralization

Inspired by mechanism of nature organisms to produce biominerals, biomimetic mineralization has been utilized to synthesize various inorganic oxides, including TiO_2.[48-50] The hydrophilic nature of TiO_2 NPs has attracted a great deal of attention due to the distinct fouling-resistant property and underwater superoleophobicity.[51] In this work, the preparation of hybrid membranes was accomplished by the polyamines induced mineralization. PVDF-g-PTA copolymer was synthesized employing PTA moiety as the mineralization inducer for titanium precursor (Fig. S1a† and S2†). The PTA chain of PVDF-g-PTA copolymer acted as the polyamine inducer to *in situ* catalyze the nucleation and growth of inorganics TiO_2 NPs from TALH precursor. The PVDF backbone of PVDF-g-PTA copolymer ensured the excellent membrane-forming properties. Quaternary ammonium chains with high content of net positive charges facilitated the *in situ* mineralization of TALH precursor in the membrane casting solution *via* the interactions with Ti-O clusters (**Scheme 2**): firstly, positively charged PTA moiety effectively concentrated negatively charged TALH precursor through the electrostatic interaction; subsequently, the concentrated precursor underwent nucleophilic substitution of the oxygen atom of Ti-OH with an adjacent Ti atom; finally, the nascent TiO_2 from the hydrolysis and polycondensation reactions aggregated into TiO_2 NPs around PTA moiety.[52-54]

Fig. 1 depicted the SEM of the cross-section morphology of PVDF-g-PTA membrane (Fig. 1a) and PVDF-g-PTA/TiO_2 hybrid membrane with theoretical TiO_2 amount of 10 wt% (Fig. 1b). The *in situ* generated TiO_2 NPs with the particle size of 50~100 nm (Fig. 1c) developed wildly dispersed micro-papillae structures in the cross-section micrograph of PVDF-g-PTA/TiO_2 hybrid membrane. The element distribution of PVDF-g-PTA/TiO_2 hybrid membrane across the thickness was measured using EDX mapping analysis (Fig. 1d). Visually the distribution of Ti and other elements was quite uniform, suggesting that the even distribution of generated TiO_2 NPs within PVDF-g-PTA/TiO_2 hybrid membrane. This could be attributed to the synergistic effect of the randomly distributed quaternary mineralization site on the matrix polymer and the compartments created by polymer network. Moreover, the generated hydrophilic TiO_2 NPs also gave rise to the decreased surface pore size due to confined chain motion or shrinkage of PVDF-g-PTA matrix by mixed nanoparticles (Fig. 1e-h). Higher surface pore density of hybrid membranes was also observed along with the content of generated TiO_2 NPs, because the pore-forming and demixing processes during phase inversion were accelerated by hydrophilic TiO_2 NPs and residual nonsolvents in membrane casting solution.[55, 56]

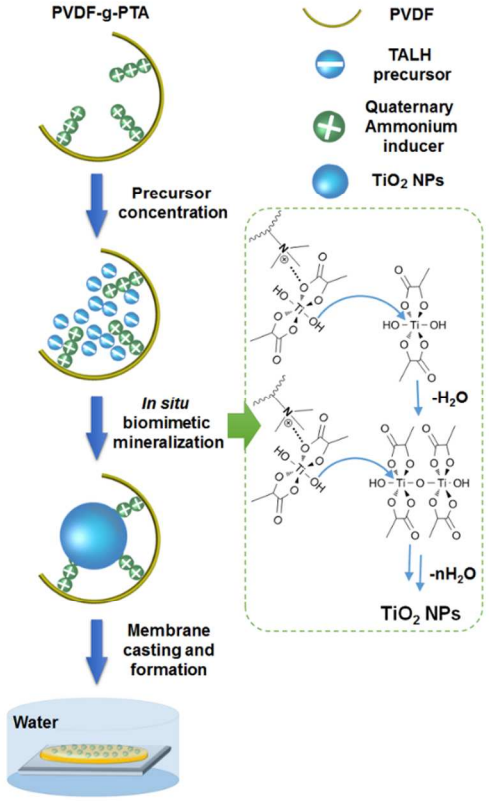

Scheme 2 Schematics of *in situ* biomimetic mineralization procedure for hybrid membranes.

Table 1 Summary of the bulk mechanical properties of PVDF-g-PTA and PVDF-g-PTA/TiO_2 hybrid membranes.

Membranes	Young's modulus (MPa)	Ultimate tensile strength (MPa)	Failure strain (%)
PVDF-g-PTA	13.0	0.408	9.41
PVDF-g-PTA/TiO_2 2.5%	17.2	0.460	11.02
PVDF-g-PTA/TiO_2 5%	23.6	0.730	27.20
PVDF-g-PTA/TiO_2 10%	39.0	0.936	16.49

As the TALH precursor dosage increased, the actual contents of *in situ* generated TiO_2 NPs in PVDF-g-PTA/TiO_2 hybrid membranes were gradually increased (Fig. S5†). The TiO_2 contents in PVDF-g-PTA/TiO_2 hybrid membranes indicated ~60% retention rate compared to that theoretically calculated from the casting solution composition. The obvious differences were due to the leaching out of both hydrophilic NPs and residual precursor during the exchange process of solvent and nonsolvent in membrane formation. With the loading of TiO_2

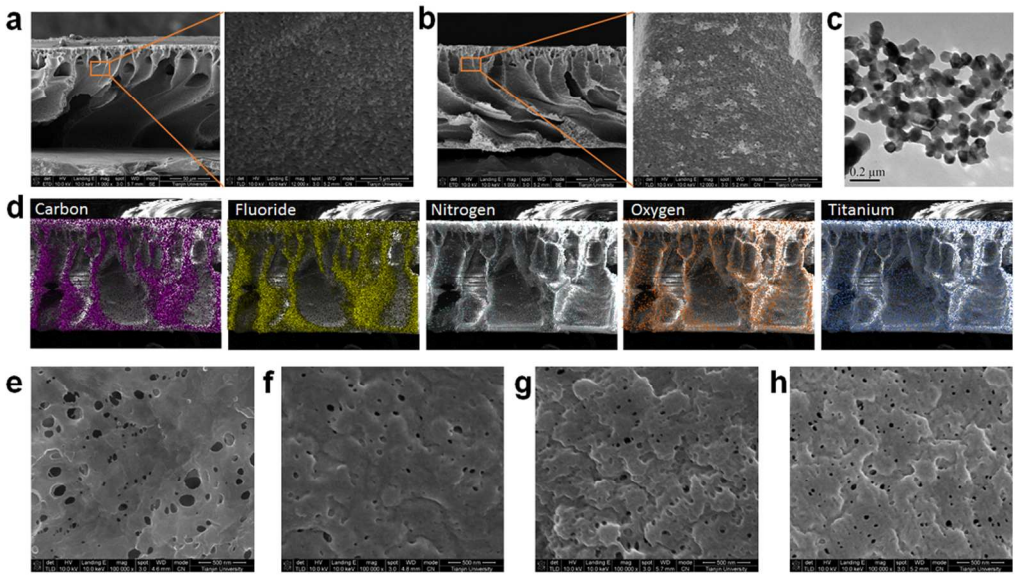

Fig. 1 SEM images of PVDF-g-PTA and PVDF-g-PTA/TiO_2 hybrid membranes. (a) Cross-section morphology of PVDF-g-PTA membrane, (b) cross-section morphology of PVDF-g-PTA/TiO_2 10% membrane, (c) TEM images of in situ generated TiO_2 NPs, (d) EDX mapping scanning spectra of C, F, N, O, and Ti elements for PVDF-g-PTA/TiO_2 10% membrane, (e) top surface morphology of PVDF-g-PTA membrane, and morphology of PVDF-g-PTA/TiO_2 hybrid membranes with theoretical TiO_2 amount of (r) 2.5 wt%, (g) 5 wt%, and (h) 10 wt%.

NPs in membranes, the mechanical properties of the hybrid membranes were simultaneously enhanced (Table 1). The Young's modulus and ultimate tensile strength of PVDF-g-PTA/TiO_2 10% membrane were increased by 200% and 129% respectively as compared to pure PVDF-g-PTA membrane. The homogenous distribution and better compatibility of TiO_2 NPs in PVDF-g-PTA/TiO_2 hybrid membranes undoubtedly avoided the no-ideal effects and inhibited the formation of interface defects.

To achieve the chemico-physical characterization of PVDF-g-PTA/TiO_2 hybrid membrane surfaces, XPS was firstly performed on the top surface of hybrid membranes. Ti was detected on the surface of PVDF-g-PTA/TiO_2 hybrid membrane (Table S1†) and the content was increased from 2.74 wt % to 7.22 wt %. The elemental compositions of Ti on the surfaces were more than twice that in the bulk, which demonstrated surface segregation of hydrophilic TiO_2 NPs driven by lowering of membrane/water interfacial free energy.[57] Higher TiO_2 NPs contents on membrane surfaces also resulted in higher hydrophilicity of membrane surfaces with a corresponding decrease in water contact angle from 76.0±1.4° to 51.4±1.3° (Fig. 2a). SFE analysis of hybrid membranes unambiguously supported surface hydrophilization (Fig. 2a): the total SFE (γ_s) and the polar (γ_s^p) components were obviously increased owing to the H-bonding interactions between water molecules and the metal-hydroxyl groups on TiO_2 surfaces. The underwater wettabilities of air and oil captive bubbles on hybrid membrane surfaces were comprehensively characterized (Fig. 2b). Each membrane was immerged in water for 24 h before measurements. The PVDF-g-PTA control membrane had relatively small underwater air-bubble contact angle of 122.4°. As a result of the gradual increase in TiO_2 content, the underwater air-bubble contact angles of hybrid membranes were increased markedly to 154.6°, indicating superhydrophilic. The underwater hexadecane contact angles also showed an increased tendency from oleophobic (115.5°) to superoleophobic (159.3°). TiO_2 induced hydrophilization was efficient for entrapping sufficient water molecules on hybrid

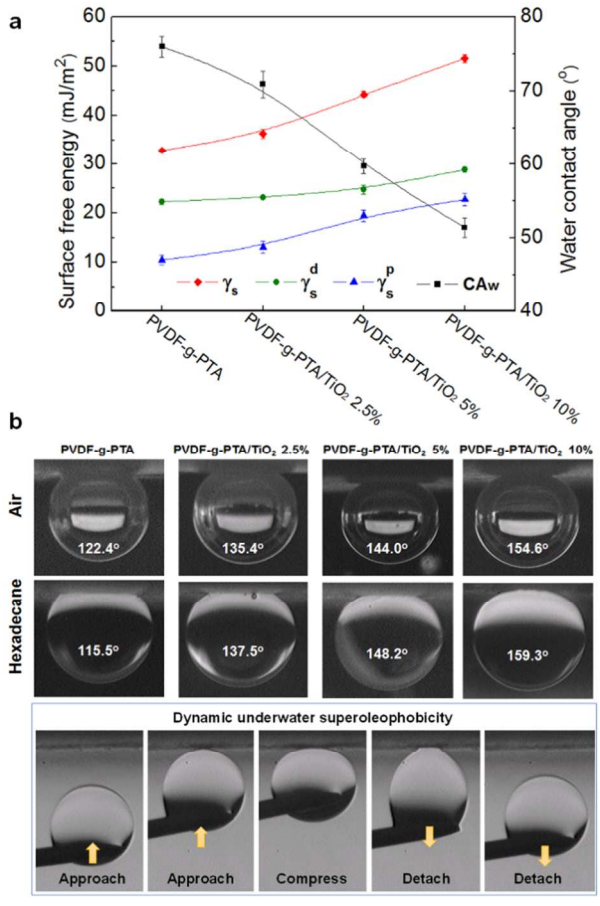

Fig. 2 (a) Water contact angles in air and the corresponding SFE parameters on PVDF-g-PTA and PVDF-g-PTA/TiO_2 hybrid membrane surfaces, (b) underwater captive air and hexadecane contact angles of PVDF-g-PTA and PVDF-g-PTA/TiO_2 hybrid membranes, and the dynamic underwater superoleophobicity (hexadecane) of PVDF-g-PTA/TiO_2 10 % hybrid membrane.

membrane surfaces to form hydration barrier layer and avoided the direct contact of oil droplets. Especially, when a hexadecane droplet was forced to contact with the hybrid membrane surface and deform the hydration barrier layer, the compressed hexadecane droplet also could be entirely removed by a needle tip, indicating dynamic underwater superoleophobicity (Fig. 2b). The durable hydrophilicity and underwater superoleophobic behavior (Fig. S6†) of PVDF-g-PTA/TiO_2 hybrid membranes would be favorable for their efficient applications in the separation of oil-in-water emulsion.

Dead-end oil-in-water emulsion separation experiments were carried out to further study the separation performance and antifouling ability of hybrid membranes. The underwater superhydrophilicity and superoleophobicity of membrane surfaces and 1~2 order of magnitude smaller pore size than oil droplet size ensured the high separation efficiency (> 99.9%) for all the membranes. Fig. 3a showed the time-dependent permeate fluxes for PVDF-g-PTA control and PVDF-g-PTA/TiO_2 hybrid membranes during the entire oil-in-water emulsion filtration process. The serious flux decline and poor flux recovery of PVDF-g-PTA control membrane was remarkably improved by TiO_2 hybridization. As the surface TiO_2 loading increased, PVDF-g-PTA/TiO_2 hybrid membranes displayed an increasing trend in flux recovery (from 57.4% to 91.6%) and a decreasing trend in flux decline (from 55.4% to 27.8%) (Fig. 3b). The hydration barrier layer constructed by hydrophilic TiO_2 microdomains on membrane surfaces contributed greatly to the anti-oil-fouling (fouling-resistant) ability of hybrid membranes (Fig. 3c).

Manipulation of Surface Heterogeneous Architecture of Hybrid Membranes

The introduction of fluoro-containing moieties (fluorinated side chain and fluoroalkyl silane) into TiO_2-based hybrid membranes aimed at constructing heterogeneous membrane surfaces with collaborative defense mechanisms. The hybrid structure rendered both organic and inorganic reaction sites for membrane modification. Based on synthetic polymer chemistry, the fluoro-containing monomer was grafted on PVDF simultaneously with quaternary ammonium monomer prior to biomimetic mineralization. During biomimetic mineralization process, the quaternary ammonium chain directed the synthesis of hydrophilic TiO_2 NPs and the fluorinated side chain induced the heterogeneousity (Fig. 4a). The as-prepared PVDF-g-PHFBM-PTA/TiO_2 hybrid membranes combined the physicochemical attributes of both polymeric and inorganic phase. Based on nano-modification chemistry, the FTS precursors were grafted on TiO_2 NPs surface after biomimetic mineralization (Fig. 4c). Hydrophilic TiO_2 NPs were generated by biomimetic mineralization and heterogeneousity was induced by coupling fluorinated silane coupling agent with Ti–OH groups. The as-prepared PVDF-g-PTA/TiO_2-FTS hybrid membranes exhibited the physicochemical attributes of heterogeneously modified NPs. No clear differences were observed in the asymmetric structures and surface morphologies of hybrid membranes after introducing fluoro-containing moieties (Fig. S7†).

XPS was performed to provide chemical information about the surface heterogeneousity of PVDF-g-PHFBM-PTA/TiO_2 and PVDF-g-PTA/TiO_2-FTS hybrid membranes. For PVDF-g-PHFBM-PTA/TiO_2 membrane, atomic C 1s, N 1s, O 1s, F 1s, and Ti 2p were present at the surface, and for PVDF-g-PTA/TiO_2-FTS hybrid membrane, atomic C 1s, N 1s, O 1s, F 1s, Ti 2p and Si 2p were present at the surface (Fig. S8†). The C 1s peak deconvolution showed six carbons with different environments, corresponding to neutral CH (284.9 eV), CH_2(PVDF, 286.1 eV), C-O (ester, 287.9 eV), C=O/C-F (289.0 eV), CF_2 (290.6 eV), CF_3 (293.5 eV) (Fig. 4b,d). The Ti 2p peak deconvolution showed two different Ti peaks of Ti $2p^{3/2}$ and Ti $2p^{1/2}$ at 459.1 eV and 465.0 eV, respectively (Fig. 4b,d, inset). These combined results verified the presence of TiO_2 microdomains and fluoro-containing microdomains on both surfaces of hybrid membranes. The quantitative analysis of the surface TiO_2 and -CF_3 contents were listed in (Fig. 4e). The surface -CF_3 contents were increased with the degree of fluorination without significant impact to the surface TiO_2 contents. With water molecules absorbed by TiO_2 microdomains, the heterogeneous membrane surfaces maintained similar underwater superhydrophilic (Fig. S9†) and superoleophobic property (Fig. 4f, inset) compare with PVDF-g-PTA/TiO_2 membrane. Higher surface -CF_3 contents resulted in dramatic decrease of SFE (Fig. 4f), which was unfavorable for oil adhesion. During the detaching process of compressed

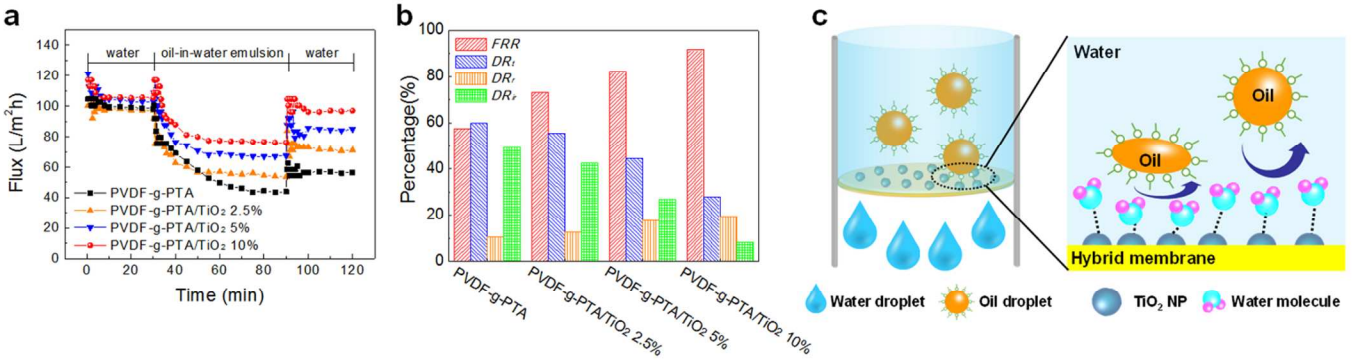

Fig. 3 (a) Time-dependent permeate fluxes for as-prepared membranes in three stage filtration: 0.5 h water filtration, 1 h oil-in-water emulsion filtration and 0.5 h water filtration after rinsing, (b) a summary of the corresponding *FRR*, DR_i, DR_r, and DR_{ir} parameters, and (c) schematic of defense mechanisms for PVDF-g-PTA/TiO_2 hybrid membranes.

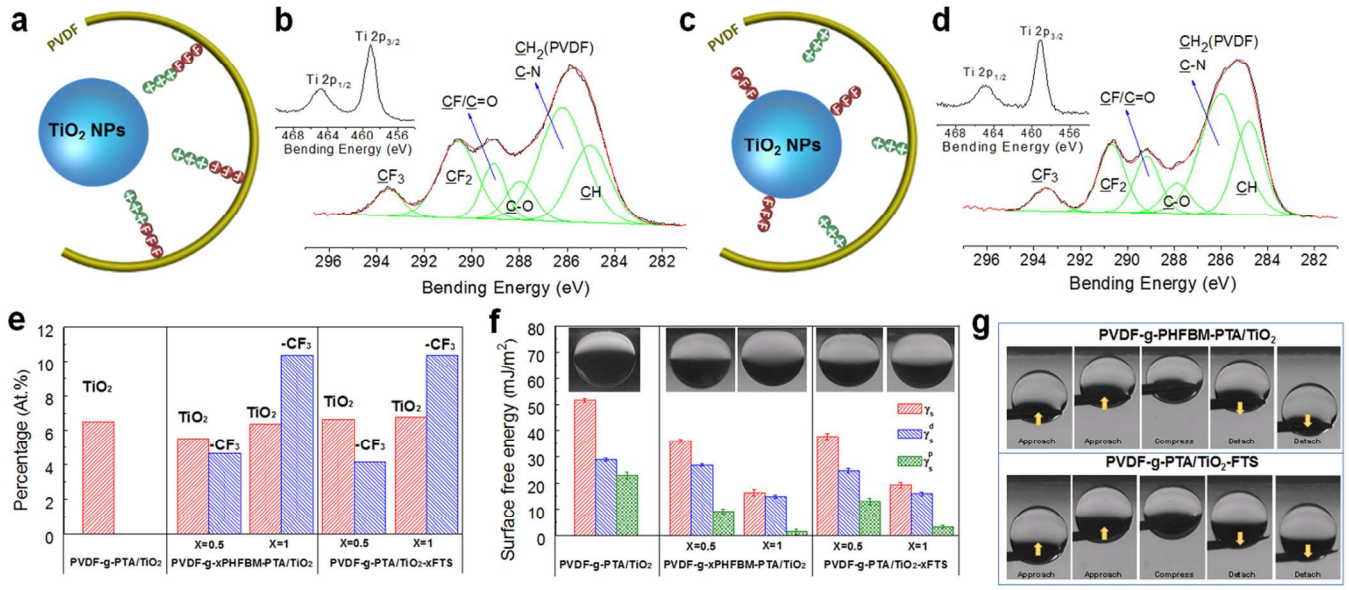

Fig. 4 Schematic for the heterogeneous structures of (a) PVDF-g-PHFBM-PTA/TiO_2 and (b) PVDF-g-PTA/TiO_2-FTS hybrid membranes. Detailed C 1s XPS spectra (inset: detailed Ti 2p XPS spectra) of (c) PVDF-g-xPHFBM-PTA/TiO_2 (x=1) and (d) PVDF-g-xPTA/TiO_2-FTS (x=1) hybrid membranes. (e) Surface chemical composition (calculated from Equation S1† and S2†) of heterogeneous membrane surfaces. (f) SFE parameters and underwater hexadecane contact angles of heterogeneous membrane surfaces. (g) Dynamic underwater superoleophobicity (hexadecane) of PVDF-g-xPHFBM-PTA/TiO_2 (x=1) and PVDF-g-PTA/TiO_2-xFTS (x=1) hybrid membrane.

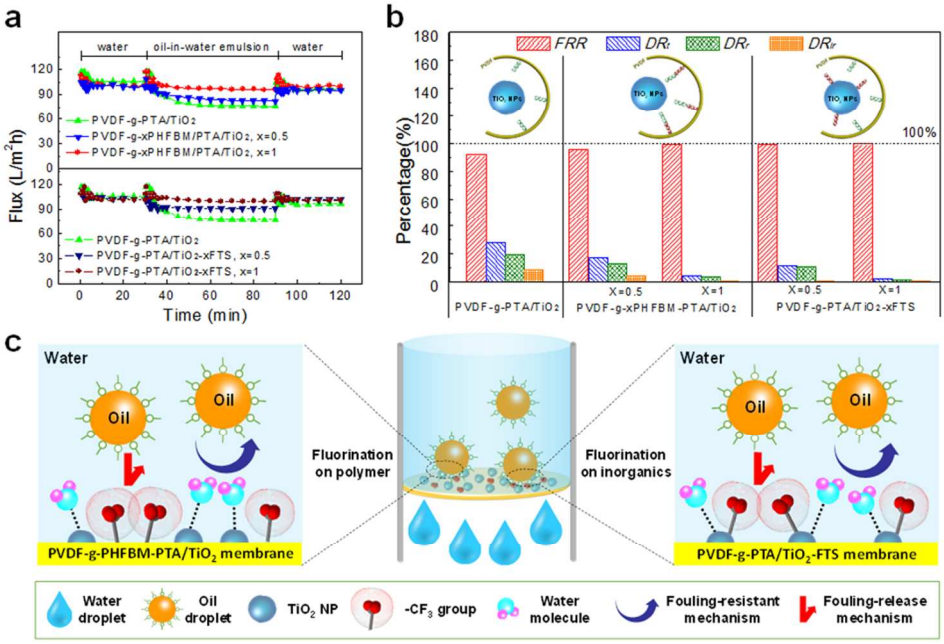

Fig. 5 (a) Time-dependent permeate fluxes for hybrid membranes in three stage filtration: 0.5 h water filtration, 1 h oil-in-water emulsion filtration and 0.5 h water filtration after rinsing, (b) a summary of the corresponding *FRR*, DR_t, DR_r, and DR_{ir} parameters, and (c) schematic of collaborative defense mechanisms for heterogeneously constructed hybrid membranes

hexadecane droplets away from membranes, no adhesion induced extensional deformation was observed on both PVDF-g-PHFBM-PTA/TiO_2 and PVDF-g-PTA/TiO_2-FTS hybrid membrane surfaces (Fig. 4g). The superhydrophilic, superoleophobic, and low adhesion properties of hybrid membranes with heterogeneous architecture on the surfaces indicated excellent anti-oil-fouling performance during the separation of oil-in-water emulsion.

As discussed above, the PVDF-g-PTA/TiO_2 hybrid membranes exhibited fouling-resistant capability by forming compact hydration barrier layer, yet existed ~20% reversible flux decline and ~9% irreversible flux decline. The goal of imparting heterogeneousity to hybrid membranes was to further incorporate LSFE, non-adhesion barrier layers and promote the release of oil foulants from membrane surfaces. Fig. 5 showed the time-dependent permeate fluxes of water and oil-in-water

emulsion for hybrid membranes. Both heterogeneously constructed hybrid membranes exhibited significant inhibition of flux decline with respect to hydrophilic PVDF-g-PTA/TiO_2 hybrid membranes. When the surface -CF_3 content reached about 10 At.% (PVDF-g-xPHFBM-PTA/TiO_2 or PVDF-g-PTA/TiO_2-xFTS, x=1), the oil fouling was minimized and no significant flux decline can be observed during oil-in-water emulsion filtration. Collaborative defense mechanisms, including fouling-resistance and fouling-release, jointly led to the remarkable enhancement in the separation performance and antifouling ability of hybrid membranes, as shown in Fig. 5c. The great hydration tendency of TiO_2 microdomains on membrane surfaces was undoubtedly responsible for the favorable interaction with water (polar liquids) in hydration barrier layers, and simultaneously, the tightly bound electron pairs of -CF_3 groups presented an unfavorable interaction with oil (nonpolar liquids) in non-adhesion barrier layers. Both factors synergistically inhibited the spreading and coalescing of the oil droplets on membrane surface and accomplished the efficient oil/water separation.

Conclusions

In summary, we have explored a novel method to fabricate hybrid membranes through the synergy of *in situ* biomimetic mineralization and nonsolvent induced phase separation for efficient oil/water separation. The as-prepared hybrid membrane demostrated the homogeneous dispersion of nanoparticles, higher mechanical strength, underwater superoleophobicity and surface heterogeneousity. The co-presence of TiO_2-bearing inorganic microdomains and fluoro-bearing organic microdomains on membrane surface endows membranes with tunable fouling-resistant and fouling-release mechanisms, which effectively prevent the oil foulants from approaching or adhering to the membrane surface. During the separation of oil-in-water emulsion, the hybrid membranes showed near zero flux decline and near complete flux recovery, demonstrating remarkably improved oil/water separation performance and superior antifouling ability. This study may set a simple and universal example to construct the hierarchical surface and manipulate the collaborative defense mechanisms for a broad range of water treatment relevant applications.

Acknowledgements

This work was supported by National Science Fund for Distinguished Young Scholars (21125627), Tianjin Natural Science Foundation (2014JCZDJC37400, 13JCYBJC20500), the Program of Introducing Talents of Discipline to Universities (No. B06006).

Notes and references

[a] Key Laboratory for Green Chemical Technology of Ministry of Education, School of Chemical Engineering and Technology, Tianjin University, Tianjin 300072, China.

[b] Collaborative Innovation Center of Chemical Science and Engineering (Tianjin), Tianjin 300072, China.

[c] Tel: 86-22-27406646; Fax: 86-22-27406646; E-mail address: zhyjiang@tju.edu.cn (Z.Y. Jiang)

† Electronic Supplementary Information (ESI) available: [Synthesis and characterizations of PVDF-g-PTA copolymer, PVDF-g-xPHFBM-PTA copolymer, and fluorinated triethoxysilane precursor. Digital photo of membrane casting solution during membrane preparation. The content analysis results for membrane bulk and surface of PVDF-g-PTA/TiO_2 hybrid membranes. Durable hydrophilicity and superoleophobicity of PVDF-g-PTA/TiO_2 hybrid membranes. SEM images, XPS spectrum and underwater wetting behavior of PVDF-g-PHFBM-PTA/TiO_2 and PVDF-g-PTA/TiO_2-FTS hybrid membranes. Calculation method of the TiO_2 and -CF_3 contents on membrane surfaces.]. See DOI: 10.1039/b000000x/

1. Y. Zhu, D. Wang, L. Jiang and J. Jin, *NPG Asia Mater.*, 2014, **6**, e101.
2. Z. Chu, Y. Feng and S. Seeger, *Angew. Chem. Int. Ed.*, 2014, DOI: 10.1002/anie.201405785.
3. Z. Xue, Y. Cao, N. Liu, L. Feng and L. Jiang, *J. Mater. Chem. A*, 2014, **2**, 2445-2460.
4. Y. Zhu, F. Zhang, D. Wang, X. F. Pei, W. Zhang and J. Jin, *J. Mater. Chem. A*, 2013, **1**, 5758-5765.
5. W. Zhang, Y. Zhu, X. Liu, D. Wang, J. Li, L. Jiang and J. Jin, *Angew. Chem. Int. Ed.*, 2014, **53**, 856-860.
6. J.-W. Lee, J. Jung, Y. H. Cho, S. K. Yadav, K. Y. Baek, H. B. Park, S. M. Hong and C. M. Koo, *ACS Appl. Mater. Interfaces*, 2014, **6**, 14600-14607.
7. A. Raza, B. Ding, G. Zainab, M. El-Newehy, S. S. Al-Deyab and J. Y. Yu, *J. Mater. Chem. A*, 2014, **2**, 10137-10145.
8. X. Zhao, Y. Su, H. Dai, Y. Li, R. Zhang and Z. Jiang, *J. Mater. Chem. A*, 2014, DOI: 10.1039/C1034TA06179A.
9. M. Tao, L. Xue, F. Liu and L. Jiang, *Adv. Mater.*, 2014, **26**, 2943-2948.
10. H.-C. Yang, K.-J. Liao, H. Huang, Q.-Y. Wu, L.-S. Wan and Z.-K. Xu, *J. Mater. Chem. A*, 2014, **2**, 10225-10230.
11. W. Chen, Y. Su, J. Peng, Y. Dong, X. Zhao and Z. Jiang, *Adv. Funct. Mater.*, 2011, **21**, 191-198.
12. X. Zhao, W. Chen, Y. Su, W. Zhu, J. Peng, Z. Jiang, L. Kong, Y. Li and J. Liu, *J. Membr. Sci.*, 2013, **441**, 93-101.
13. W. Chen, Y. Su, J. Peng, X. Zhao, Z. Jiang, Y. Dong, Y. Zhang, Y. Liang and J. Liu, *Environ. Sci. Technol.*, 2011, **45**, 6545-6552.
14. X. Zhu, H.-E. Loo and R. Bai, *J. Membr. Sci.*, 2013, **436**, 47-56.
15. L. Zhang, Z. Zhang and P. Wang, *NPG Asia Mater.*, 2012, **4**, e8.
16. J. Gu, P. Xiao, J. Chen, J. Zhang, Y. Huang and T. Chen, *ACS Appl. Mater. Interfaces*, 2014, **6**, 16204-16209.
17. B. D. McCloskey, H. B. Park, H. Ju, B. W. Rowe, D. J. Miller and B. D. Freeman, *J. Membr. Sci.*, 2012, **413–414**, 82-90.
18. J. Jin, J. S. Gao, Y. Zhu and F. Zhang, *J. Mater. Chem. A*, 2014, DOI: 10.1039/C1034TA05624H.
19. K. Zhou, Q. G. Zhang, H. M. Li, N. N. Guo, A. M. Zhu and Q. L. Liu, *Nanoscale*, 2014, **6**, 10363-10369.
20. F. Zhang, W. B. Zhang, Z. Shi, D. Wang, J. Jin and L. Jiang, *Adv. Mater.*, 2013, **25**, 4192-4198.
21. P. C. Chen and Z. K. Xu, *Sci. Rep.*, 2013, **3**.
22. P. Gao, Z. Liu, D. D. Sun and W. J. Ng, *J. Mater. Chem. A*, 2014, **2**, 14082-14088.

23. S. J. Gao, Z. Shi, W. B. Zhang, F. Zhang and J. Jin, *ACS Nano*, 2014, **8**, 6344-6352.
24. H.-C. Yang, J.-K. Pi, K.-J. Liao, H. Huang, Q.-Y. Wu, X.-J. Huang and Z.-K. Xu, *ACS Appl. Mater. Interfaces*, 2014, **6**, 12566-12572.
25. S. Yang, Y. Si, Q. Fu, F. Hong, J. Yu, S. S. Al-Deyab, M. El-Newehy and B. Ding, *Nanoscale*, 2014, **6**, 12445-12449.
26. Y. Dong, J. Li, L. Shi, X. Wang, Z. Guo and W. Liu, *Chem. Commun.*, 2014, **50**, 5586-5589.
27. H. Li, Y. Huang, Y. Mao, W. L. Xu, H. J. Ploehn and M. Yu, *Chem. Commun.*, 2014, **50**, 9849-9851.
28. Y. Huang, H. Li, L. Wang, Y. Qiao, C. Tang, C. Jung, Y. Yoon, S. Li and M. Yu, *Adv. Mater. Interfaces*, 2014, DOI: 10.1002/admi.201400433.
29. A. K. Kota, G. Kwon, W. Choi, J. M. Mabry and A. Tuteja, *Nat. Commun.*, 2012, **3**, 1025.
30. K. Liu and L. Jiang, *Annu. Rev. Mater. Res.*, 2012, **42**, 231-263.
31. Y. Tian, B. Su and L. Jiang, *Adv. Mater.*, 2014, **26**, 6872-6897.
32. D. F. Cheng, B. Masheder, C. Urata and A. Hozumi, *Langmuir*, 2013, **29**, 11322-11329.
33. A. M. Coclite, Y. Shi and K. K. Gleason, *Adv. Mater.*, 2012, **24**, 4534-4539.
34. J. Zhao, X. Zhao, Z. Jiang, Z. Li, X. Fan, J. Zhu, H. Wu, Y. Su, D. Yang, F. Pan and J. Shi, *Prog. Polym. Sci.*, 2014, **39**, 1668-1720.
35. C. Li and D. L. Kaplan, *Curr. Opin. Solid State Mater. Sci.*, 2003, **7**, 265-271.
36. N. A. J. M. Sommerdijk and M. Cusack, *Nat. Mater.*, 2014, **13**, 1078-1079.
37. M. B. Dickerson, K. H. Sandhage and R. R. Naik, *Chem. Rev.*, 2008, **108**, 4935-4978.
38. C. M. Lukehart, Scott, R. A, *Nanomaterials: Inorganic and Bioinorganic Perspectives*, John Wiley & Sons, New York, 2008.
39. A.-W. Xu, Y. Ma and H. Colfen, *J. Mater. Chem.*, 2007, **17**, 415-449.
40. K. Gorna, R. Muñoz-Espí, F. Gröhn and G. Wegner, *Macromol. Biosci.*, 2007, **7**, 163-173.
41. F. Pan, Q. Cheng, H. Jia and Z. Jiang, *J. Membr. Sci.*, 2010, **357**, 171-177.
42. P. Calvert and P. Rieke, *Chem. Mater.*, 1996, **8**, 1715-1727.
43. S. Kango, S. Kalia, A. Celli, J. Njuguna, Y. Habibi and R. Kumar, *Prog. Polym. Sci.*, 2013, **38**, 1232-1261.
44. Y. Xiong, Q. L. Liu, A. M. Zhu, S. M. Huang and Q. H. Zeng, *Journal of Power Sources*, 2009, **186**, 328-333.
45. B. Li, W. Liu, H. Wu, S. Yu, R. Cao and Z. Jiang, *J. Membr. Sci.*, 2012, **415–416**, 278-287.
46. H. Mori, C. Sada, T. Konno and K. Yonetake, *Polymer*, 2011, **52**, 5452-5463.
47. D. K. Owens and R. C. Wendt, *J. Appl. Polym. Sci.*, 1969, **13**, 1741-1747.
48. J. L. Sumerel, W. Yang, D. Kisailus, J. C. Weaver, J. H. Choi and D. E. Morse, *Chem. Mater.*, 2003, **15**, 4804-4809.
49. Z. Tong, Y. Jiang, D. Yang, J. Shi, S. Zhang, C. Liu and Z. Jiang, *RSC Adv.*, 2014, **4**, 12388-12403.
50. S. H. Yang, K. Kang and I. S. Choi, *Chem. Asian J.*, 2008, **3**, 2097-2104.
51. K. Liu, M. Cao, A. Fujishima and L. Jiang, *Chem. Rev.*, 2014, **114**, 10044-10094.
52. X. Liu, Y. Gao, C. Cao, H. Luo and W. Wang, *Langmuir*, 2010, **26**, 7671-7674.
53. S. L. Sewell and D. W. Wright, *Chem. Mater.*, 2006, **18**, 3108-3113.
54. Y. Yan, B. Hao, X. Wang and G. Chen, *Dalton Trans.*, 2013, **42**, 12179-12184.
55. P. Sukitpaneenit and T.-S. Chung, *J. Membr. Sci.*, 2009, **340**, 192-205.
56. L.-J. Zhu, L.-P. Zhu, J.-H. Jiang, Z. Yi, Y.-F. Zhao, B.-K. Zhu and Y.-Y. Xu, *J. Membr. Sci.*, 2014, **451**, 157-168.
57. H. Kuroki, I. Tokarev, D. Nykypanchuk, E. Zhulina and S. Minko, *Adv. Funct. Mater.*, 2013, **23**, 4593-4600.

Journal of Materials Chemistry A RSCPublishing

ARTICLE

Table of contents entry:

Antifouling hybrid membranes were prepared through the synergy of *in situ* biomimetic mineralization and nonsolvent induced phase separation, which endows membrane surfaces with collaborative defense mechanisms.